

# A novel type-2 fuzzy logic controller based hybrid micro grid with different renewable energy resources

Achammagari Leelendra Prasad, Guriginjakunta Maheswara Naidu, Konathapalle Jaswanth, Atla Jaswanth, B.Murali Mohan,

*Annamacharya Institute of Technology And Sciences, Rajampeta,  
M.Tech(Assistant Professor)*

G. Soundarya, C. K. Sundarabalan, C. Balasundar, D. Karthikaikannan, and Jayant Sharma, R. Sitharthan

*School of EEE, SASTRA Deemed University, Thanjavur 613401, India  
Department of EEE, VIT, Vellore 632014, India*

Date of Submission: 12-03-2023

Date of Acceptance: 22-03-2023

**ABSTRACT**— The increased demand and depletion of the fossil fuels for power generation led to the need for extracting power from the renewable energy resources (RERs). The microgrids (MGs) are redesigned with the help of effective power extracted from renewable sources such as solar, wind, tidal, and geothermal. The advent of DCMGs overcomes the conventional AC grids. The hybridization of the AC and DCMGs will provide more advantages for various levels of consumers. This article proposes the design and modeling of a hybrid DC/ACMG with the efficient use of RERs and it can reduce numerous power conversions. The solar energy is extracted through photovoltaic (PV) panels meritoriously using interval type 2 fuzzy logic technique as the maximum power point tracking algorithm. The AC grid is designed using wind energy source and tidal energy. The permanent magnet synchronous generator is used as the wind turbine. Various control mechanisms are employed in order to extract maximum power from the wind and tidal waves at varying conditions. These generated powers can supply the load and are connected to the utility grid. These are executed with the aid of MATLAB/SIMULINK software.

**Index Terms**— Hybrid DC/AC microgrid (MG), permanent magnet synchronous generator, power extraction,

solar photovoltaic (PV) energy, tidal energy, wind energy.

## I. INTRODUCTION

The generating sources close to the load take advantage of reducing transmission losses and preventing network congestion [1]. Different generating sources such as wind, solar, fuel cell, and tidal and energy storage devices such as battery and flywheel are connected to a common network which is said to be known as microgrid (MG) [2]. The growth of DC loads in the distribution side such as light-emitting diode lights, electric vehicles, laptops, and uninterruptible power supply makes a major concern about hybrid AC/DC MG to reduce the complexity and power conversion stages. AC, DC, and hybrid MG control techniques are reviewed in [3]. A neural network control-based grid-connected hybrid AC/DCMG is presented in [4]. The wind, solar, fuel cell, and batteries are utilized as a generating and storage system. A fault-tolerant supervisory controller is designed for isolated hybrid AC/DCMG in [5], and it satisfies the power demand in both AC and DC MG. The work in [6] presents the coordinated control strategy for isolated wind-diesel hybrid MG to reduce the frequency deviation resulting from

renewable energy fluctuation and load variance. The topology of hybrid AC/DC MG based on the conventional power network and the interconnection of the AC and DC networks are reviewed in [2]. A bidirectional resonant DC transformer is implemented in [7] to replace the conventional bulky transformer for bus voltage matching and the galvanic isolation in a hybrid MG. An architecture and control for multiple MGs with a hybrid AC/DC connection is designed in [8]. A detailed model of automatic centralized MG controller-based hybrid AC/DC MG is presented in [9]. The technologies, key drivers, and outstanding issues of MG are reviewed in [10]. Different control methods and controllers are used for maximum power point tracking (MPPT) in solar photovoltaic (PV), wind, and the other renewable energy-based power-generating systems. A radial basis function network-based MPPT control algorithm for a hybrid solar and wind energy system is designed and analyzed in [11] for standalone and grid-connected applications. Keyrouz and Fakheredine [12] presented the machine learning control-based MPPT for PV system under partial shading condition. The Perturb & Observe (P&O)-based fractional-order sliding-mode controller for MPPT of the PV system is designed in [13]. A decentralized dynamic power-sharing method for wind, PV, and

the solar irradiation and temperature [17]. The PV modules are connected in series and parallel combinations to get the required power output [18]. The number of PV modules to be connected in series  $N_s$  can be determined from

$$N_s = \frac{V_{DClink}}{V_{MP}} \quad (1)$$

where  $V_{DClink}$  is the DC link voltage and  $V_{MP}$  is the voltage at the maximum power point (MPP) of the PV module.

The PV string maximum power  $P_{String}$  connected in series is

$$P_{String} = N_s \cdot P_{MP} \quad (2)$$

$$P_{MP} = V_{MP} \cdot I_{MP} \quad (3)$$

The number of strings to be connected in parallel  $N_p$  is

$$N_p = \frac{P_t}{P_{String}} \quad (4)$$

where  $P_{MP}$  is the power at MPP,  $I_{MP}$  is the current at MPP, and  $P_t$  is the needed total power from the PV module.

### C. Modeling of Wind Turbine Generator

The mechanical power that can be extracted from the WT is given in the following equation [20], [21]:

$$P_m = \frac{1}{2} \rho A_r C_p(\lambda, \beta) V^3 \quad (5)$$

## II. SYSTEM MODELING AND CONFIGURATION

### A. Hybrid DC/AC Microgrid

The mechanical torque output

$T_m$  is expressed in the following equation:

$$T_m = \frac{P_m}{\omega_m} = \frac{1}{2} \frac{\rho A_r C_p(\lambda, \beta) V^3}{\omega_m} \quad (6)$$

The fundamental scheme of a hybrid DC/AC MG is shown in Fig. 1. It comprises DC grid and AC grid interlinked by a bidirectional DC/AC converter. The DC MG comprises PV panels system and a battery bank storage system. The DC loads are reconnected to the DCMG via DC bus. The AC MG comprises the wind turbine (WT) system and tidal turbines system. This system is tied to the utility grid, where  $\rho$  is the air density ( $\text{kg/m}^3$ ),  $A_r$  represents the area swept by the rotor,  $C_p$  is the power coefficient,  $V_w$  represents the wind velocity (m/s),  $\lambda$  is the tip speed ratio,  $\beta$  is the pitch angle (deg),  $\omega_R$  is the angular velocity (rad/s), and  $R$  is the blade radius (m). Fig. 2 shows the schematic of PMSG WT.

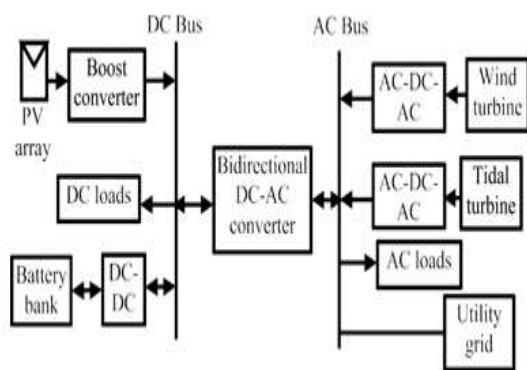


Fig. 1. Fundamentals scheme of a hybrid DC/AC MG.

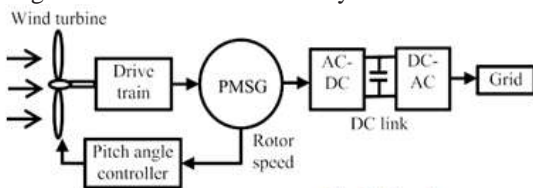


Fig. 2. Schematic of PMSG WT.

### B. Modeling of PV Panel

The PV model output mainly depends on

Usingd-

$$\frac{di_d}{dt} = \frac{-R_s I_d + L_q \rho \omega_r i_q + V_d}{L_d} \quad (7)$$

$$\frac{di_q}{dt} = \frac{-R_s I_q - L_d \rho \omega_r i_d - p \lambda_a \omega_r + V_q}{L_q} \quad (8)$$

$$T_n = 0.75 p (\lambda_a + (L_d - L_q) i_d i_q) \quad (9)$$

where  $L_q$  is the q-axis inductance,  $L_d$  is the d-axis inductance,  $R_s$  is the resistance of the stator windings,  $i_q$  is the q-axis current,  $i_d$  is the d-axis current,  $V_q$  is the q-axis voltage,  $V_d$  is the d-axis voltage,  $\omega$  is the angular velocity of the rotor,  $\lambda_a$  is the amplitude of flux induced, and  $p$  is the number of pole pairs.

#### D. Modeling of Drive Train

In the two-mass model, the masses of the two disks are added. These two disks are connected by a shaft of equivalent stiffness [22]. The disk's mass moment of inertia  $J$  ( $\text{kg} \cdot \text{m}^2$ ) is given by the following equation:

$$J = \frac{MD^2}{8} \quad (10)$$

where  $D_d$  is the disk diameter and  $M$  is the disk weight. The shaft stiffness  $K_s$  ( $\text{N} \cdot \text{m/rad}$ ) is determined by the following equation:

$$K_s = \frac{G \pi D_s^4}{32 L_s} \quad (11)$$

where  $D_s$  is the diameter of the shaft,  $L_s$  is the length of the shaft, and  $G$  is the shear modulus. The two-mass model drive train is used in this article and it is modeled as follows:

$$J \frac{d\omega_g}{dt} = T_n - T_e - V_f \omega_g \quad (12)$$

where  $T_n$  is the mechanical torque,  $T_e$  is the electromagnetic torque of generator,  $J$  is the rotating mass inertia constant, and  $\omega_g$  is the angular speed of the rotor.

E. Modeling of Tidal Stream Energy Generation System Fig. 3 shows the block diagram of the tidal stream energy generation system (TSEGS). It consists of a horizontal axis tidal turbine (HATT) which captures the kinetic energy (KE) of the tidal wave [23], [24]. The PMSG is used to convert it into electrical energy. The AC is converted into DC and transmitted to the land where DC-AC conversion is made and connected to the grid through a step-up transformer [25]. The density of water is 784 times greater than air. With small turbines at low tidal speeds, an enormous amount of power can be generated when compared with WT [26]. The HPTT will produce 4-5 times of power higher than the WT with an analogous turbine rating. The KE onto the tidal turbine

reference, the model of PMSG is given as follows: produces a total power [25] as given in the following equation:

$$P_{total} = \frac{1}{2} \rho \pi R^3 C_p(\lambda, \theta) V^3 \quad (13)$$

where  $\rho$  is the fluid density ( $\text{kg/m}^3$ ),  $V$  is the tidal velocity (m/s),  $R$  is the radius of the blade (m),  $C_p$  is the power coefficient,  $\lambda$  is the tip speed ratio, and  $\theta$  is the pitch angle (degree).

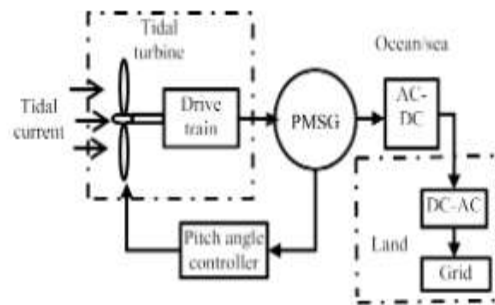


Fig.3. Block diagram of the TSEGS.

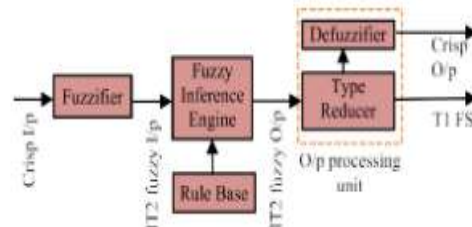


Fig.4. Flow diagram of IT2FLC.

### III. DESIGN OF THE HYBRID DC/AC MICRO GRID

The design structure of the hybrid DC/AC MG is segmented as DC MG and AC MG.

#### A. Design of DC Microgrid

The PV system contributes the necessary power to the DC MG. The next-generation thin-film solar cells are the conspicuous hope [18]. The CIGS solar cell which is very lightweight, thin, and flexible and has a very high absorption is used in this article for the design of PV array. The solar Frontier SF-170S panel, which has the highest efficiency of 19.9%, is used. In order to extract utmost and effective power from the PV system, the MPPT technique is used.

#### B. Interval Type 2 Fuzzy Logic Controller MPPT Technique for PV System

Conventionally, P&O method is used as the MPPT technique. The T1 FLC MPPT technique is also used for the PV system contribution from artificial intelligence. However, the IT2 FLC [27]

works more effectively in handling the imprecise data when compared with P&O and T1FLC. In T1FLC, the membership values are single, while the membership functions of IT2FLC are intervals instead of a single value. The MFs of IT2FLC has lower (L) and upper (U) regions. The IT2FLC has an additional step of type reduction (TR). This TR helps in reducing the IT2 fuzzy sets into IT1 fuzzy sets. The flow diagram of IT2FLC is depicted in Fig. 4.

The E and CE are divided into three fuzzy sets each.

The MFs of E and CE are shown in Fig. 5. The E and CE MFs are chosen as trapezoidal MFs for providing accurate results. The MFs are depreciate (D), neutral (NT), and appreciate (A). The output (D) is the duty cycle and it is given to the DC-DC converter. The output MFs are depreciate huge (DH), depreciate tiny (DT), NT, appreciate tiny (AT), and appreciate huge (AH). The IT2FLC uses the rule base of Table I.

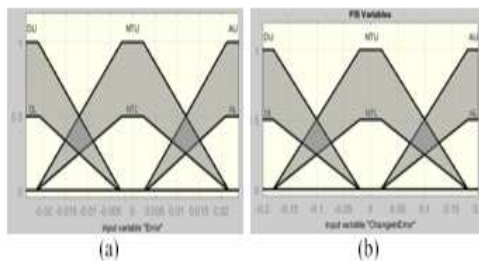


Fig. 5. MFs of IT2FLC. (a) Error. (b) Change in error.

TABLE I  
 RULE BASE FOR THE IT2FLC MPPT

E	CE		
	D	NT	A
D	DH	DT	NT
NT	DT	NT	AT
A	NT	AT	AH

The 270 V produced by the PV array is boosted to 500-VDC using this Boost converter. The duty cycle is automatically varied with the help of the MPPT structure. A total load of 30 kW is used in the DC MG. The 20-kW load is the permanent residential load. At peak time, there is a load hike of 10 kW. A 40-Ah Li-ion battery bank system is used to store the power. When the power production is insufficient by PV arrangement, the battery bank supplies the residential load. The battery model is referred in [19].

### C. Design of AC Microgrid

A wind energy conversion system

(WECS) consisting of a 100-kW WT and a TSEGS of 50 kW forms the AC MG and is also connected to the utility grid. It consists of a synchronous generator connected to an AC/DC converter, a DC link, and a DC/AC IGBT-based pulse width modulation (PWM) converter. The tip speed ratio is maintained at the optimum value. Therefore, the power extraction coefficient  $C_p$  is also at the optimum value. Speed regulator and pitch angle control techniques are used. Therefore, MPPT is tracked continuously, and the power is produced effectively and efficiently. The critical hospital load of 40 kW is coupled to the AC MG. The power interruption for a few minutes can harm the patients' life. Failure of either of the system does not affect the power supplied to the hospital.

### D. Design of Bidirectional DC/AC Converter

Converters play an important role in the synchronization process. The bidirectional DC/AC converter is an online converter which is common between the DC bus and the AC bus. It allows the bidirectional flow of power between DC bus and AC bus. It can work both as an inverter and as a rectifier. When there is a power deficit in the DC MG, the converter works as a rectifier and power is supplied from the AC side to the DC MG, thereby preventing the isolation of the loads connected to the DC bus. The voltage source control technique is used which has precise control over the magnitude, phase, and frequency of the voltage. The bypass diodes which are anti-parallel to the switches help in the circulation of active

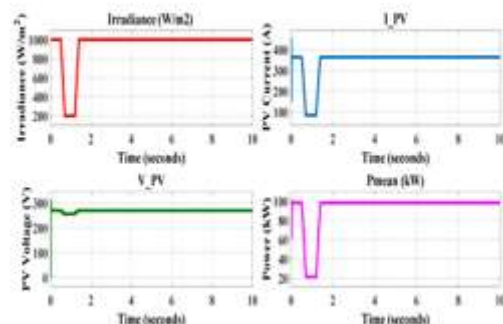


Fig. 6. PV output using IT2FLC MPPT at varying irradiance conditions.



TABLE II  
 PERFORMANCE OF PV SYSTEM WITH  
 VARIOUS MPPT TECHNIQUES

Parameters	P&O	T1FLC	IT2FLC
Output power at 1000 W/m <sup>2</sup>	90.95 kW	96.18 kW	98.29 kW
Output power at 200 W/m <sup>2</sup>	16.83 kW	20.85 kW	21.86 kW
Voltage and Current	Oscillating and Non-Uniform	Smooth and Uniform	Smooth and Uniform

power and in the flow of active power in both the directions. The sinusoidal pulsewidth modulation technique is used as the switching scheme. Even if the whole ACMG fails, the hospital load will be provided with uninterrupted supply of power from the DCMG via bidirectional DC/AC converter.

#### IV. SIMULATION AND RESULTS

##### A. DC Microgrid

The CIGS solar PV array of 100 kW has an irradiation level of 1000 W/m<sup>2</sup> at 0–0.5 s. At 0.5 s, the irradiation level decreases to 200 W/m<sup>2</sup>. An average constant temperature of 35 °C is maintained. Again at 1.2 s, the irradiation level reaches 1000 W/m<sup>2</sup>.

Fig. 6 shows the PV system output using the IT2FLC MPPT technique. From 0.5 to 1.6 s, the battery bank supplies the load as the power produced by the PV is insufficient to meet the load of 30 kW. After 1.6 s, the PV again supplies the load. Table II shows the assessment of the performance of PV system with various MPPT techniques.

The above results prove that the PV system with IT2FLC MPPT technique produces utmost power than the P&O and T1FLC techniques. The power production under the minimum irradiation condition of 200 W/m<sup>2</sup> is comparatively higher in IT2FLC than the other techniques.

##### B. AC Microgrid

The AC MG is designed with RERs such as wind energy and tidal energy. PMSG outshines conventional WECS with doubly fed induction generator (DFIG) by extracting more power. PMSG has reduced losses as it does not require gear box and brushes. So, its weight is less, low losses, low noise, and less maintenance. PMSG is used in both the systems in order to extract utmost power. A total load of 40 kW is connected to the ACMG. The hospital load of 40 kW is coupled in the AC

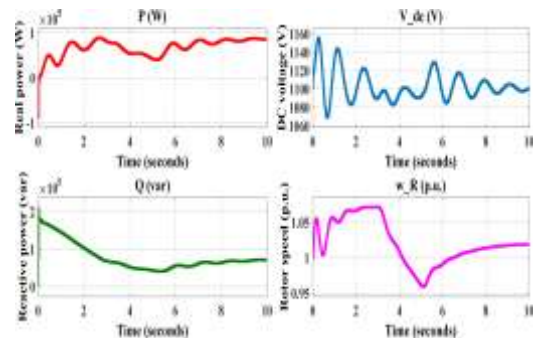


Fig. 7. Active power, reactive power, DC voltage, and rotor speed of the WT.

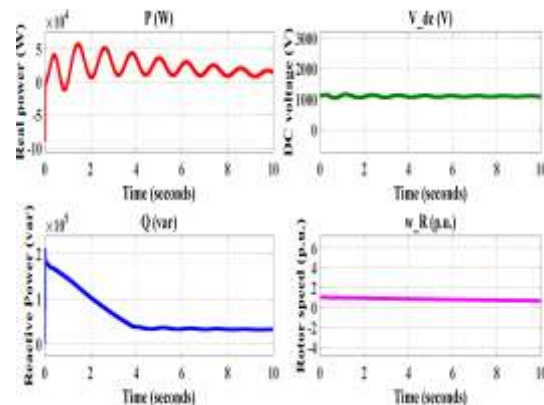


Fig. 8. Active and reactive power, DC voltage, and rotor speed of the TSEGS.

MG. The hospital load is a critical load where power supply should not be interrupted. This hybrid DC/AC MG is unique from other MGs by providing uninterrupted power supply at any cause. When the WECS does not provide enough power, the TSEGS supply the power to the hospital and vice versa. The hospital load consumes 30-kW power and during peak time, there is a hike in power consumption by 10k.

##### C. Wind Energy Conversion System

The WECS consists of PMSG WT of 100 kW, which produces power at varying wind speed conditions. Based on the yearly data, there are variations in wind speed from 15 to 5 m/s. The simulation is carried out with varying wind speed. Fig. 7 shows the active power, reactive power, DC voltage, and rotor speed of the WT. The wind speed varies from 12 to 7 m/s at 3 s. In 5 s, the wind speed again changes to 12 m/s and accordingly, the power generation varies. The rotor speed decreases when the wind speed decreases. Therefore, the power generation also reduces. The WECS with PMSG produces 50-kW power even when the wind speed is reduced to 7 m/s. When compared with DFIG, the power production is more in

WECS with PMSG. It is evident from the simulation that WECS alone will be able to supply hospital load when tidal stream energy conversion system (TSECS) is disconnected.

#### D. Tidal Stream Energy Conversion System

HATT with the generator as PMSG is used to extract most power from the tidal waves with high efficiency. A 50-kW TSEGS produce the power at an average tidal speed of 2.5 m/s. Fig. 8 shows the active power, reactive power, DC voltage, and rotor speed of the TSEGS.

The rotor speed maintains constant 1 p.u. and the power generation is also constantly produced. The power production in PV and WECS can be severely affected as it depends on varying conditions of solar irradiation and wind speed. However, the TSEGS depends on the gravitational force of the sun and moon. The power production from TSEGS is persistent which prevents the isolation of hospital load and residential load via a bidirectional converter. This makes the proposed hybrid DC/AC MG unique as it ensures the prevention of load isolation at any cause with the aid of TSEGS.

#### V. CONCLUSION

The deployment of DC loads requires the direct DC supply to reduce the conversion losses. So, this article proposed the DC/AC hybrid MG with RERs. This system is designed and modeled in the MATLAB/Simulink environment. The solar PV system and batteries are connected to the DC grid and in the AC grid, wind and tidal power generation systems are connected. The bidirectional converter is employed to exchange power from DC grid to AC grid and vice versa. An IT2FLC-based MPPT is proposed for the CIGS solar PV system. Moreover, the PMSG is used for both wind and tidal power generation systems due to its merits. The proposed system is the ultimate solution for the problems of isolation of loads and power production from non-exhaustible sources. It helps to provide electricity even in remote, isolated areas and meet the increased advent of DC loads with minimal losses. With proper design, coordination between the DC and AC MGs and control over it can effectively utilize the power generated from the RERs. The mitigation of power quality issues that arises due to the critical and sensitive hospital load and compensation of reactive power are considered as the future work.

#### REFERENCES

[1]. C. Wan et al., "A highly integrated and reconfigurable

- microgrid test bed with hybrid distributed energy sources," *IEEE Trans. Smart Grid*, vol. 7, no. 1, pp. 451–459, Jan. 2016.
- [2]. Unamuno and J. A. Barrena, "Hybrid AC/DC microgrids—Part I: Review and classification of topologies," *Renew. Sustain. Energy Rev.*, vol. 52, pp. 1251–1259, Dec. 2015.
- [3]. S. K. Sahoo, A. K. Sinha, and N. K. Kishore, "Control techniques in AC, DC, and hybrid AC–DC microgrid: A review," *IEEE J. Emerg. Sel. Topics Power Electron.*, vol. 6, no. 2, pp. 738–759, Jun. 2018.
- [4]. N. Chettibi, A. Mellit, G. Sulligoi, and A. M. Pavan, "Adaptive neural network-based control of a hybrid AC/DC microgrid," *IEEE Trans. Smart Grid*, vol. 9, no. 3, pp. 1667–1679, May 2018.
- [5]. M. Hosseinzadeh and F. R. Salmasi, "Fault-tolerant supervisory controller for a hybrid AC/DC micro-grid," *IEEE Trans. Smart Grid*, vol. 9, no. 4, pp. 2809–2823, Jul. 2018.
- [6]. M. Yuan, Y. Fu, Y. Mi, Z. Li, and C. Wang, "The coordinated control of wind-diesel hybrid micro-grid based on sliding mode method and load estimation," *IEEE Access*, vol. 6, pp. 76867–76875, 2018.
- [7]. J. Huang, J. Xiao, C. Wen, P. Wang, and A. Zhang, "Implementation of bidirectional resonant DC transformer in hybrid AC/DC micro-grid," *IEEE Trans. Smart Grid*, vol. 10, no. 2, pp. 1532–1542, Mar. 2019.
- [8]. P. Wu, W. Huang, N. Tai, and S. Liang, "A novel design of architecture and control for multiple microgrids with hybrid AC/DC connection," *Appl. Energy*, vol. 210, pp. 1002–1016, Jan. 2018.
- [9]. P. G. V. Peri, P. Paliwal, and F. C. Joseph, "AC/DC-based hybrid AC/LVDC micro-grid," *IET Renew. Power Gener.*, vol. 11, no. 4, pp. 521–528, Mar. 2017.
- [10]. A. Hirsch, Y. Parag, and J. Guerrero, "Microgrids: A review of technologies, key drivers, and outstanding issues," *Renew. Sustain. Energy Rev.*, vol. 90, pp. 402–411, Jul. 2018.
- [11]. K. Kumar, N. R. Babu, and K. R. Prabhu, "Design and analysis of RBFN-based single MPPT controller for hybrid solar and wind energy system," *IEEE Access*, vol. 5, pp. 1530

- 8–15317,2017.
- [12]. Keyrouz, “Enhanced Bayesian based MPPT controller for PV systems,” *IEEE Power Energy Technol. Syst. J.*, vol. 5, no. 1, pp. 11–17, Mar. 2018.
- [13]. B. Yang et al., “Perturbation observer based fractional-order sliding-mode controller for MPPT of grid-connected PV inverters: Design and real-time implementation,” *Control Eng. Pract.*, vol. 79, pp. 105–125, Oct. 2018.
- [14]. P. Avirajamanjula, S. Palaniyappa, and S. Ezhilarasan, “An optimal power and energy management by hybrid energy storage systems in microgrids,” *Int. J. Appl. Eng. Res.*, vol. 13, pp. 9131–9136, 2018.
- [15]. X. Li, H. Wen, Y. Hu, and L. Jiang, “A novel beta parameter based fuzzy-logic controller for photovoltaic MPPT application,” *Renew. Energy*, vol. 130, pp. 416–427, Jan. 2019.
- [16]. M. Arsalan, R. Iftikhar, I. Ahmad, A. Hasan, K. Sabahat, and A. Javeria, “MPPT for photovoltaic system using nonlinear backstepping controller with integral action,” *Sol. Energy*, vol. 170, pp. 192–200, Aug. 2018.
- [17]. M. G. Villalva, J. R. Gazoli, and E. R. Filho, “Comprehensive approach to modeling and simulation of photovoltaic arrays,” *IEEE Trans. Power Electron.*, vol. 24, no. 5, pp. 1198–1208, May 2009.
- [18]. D.-L. Popa, M.-S. Nicolae, P.-M. Nicolae, and M. Popescu, “Design and simulation of a 10 MW photovoltaic power plant using MATLAB and Simulink,” in *Proc. IEEE Int. Power Electron. Motion Control Conf. (PEMC)*, Varna, Bulgaria, Sep. 2016, pp. 378–383.
- [19]. A. Serpi, M. Porru, and A. Damiano, “An optimal power and energy management by hybrid energy storage systems in microgrids,” *Energies*, vol. 10, no. 11, p. 1909, 2017.
- [20]. A. Rolán, Á. Luna, G. Vázquez, D. Aguilar, and G. Azevedo, “Modeling of a variable speed wind turbine with a permanent magnet synchronous generator,” in *Proc. IEEE Int. Symp. Ind. Electron. (ISIE)*, Jul. 2009, pp. 734–739.
- [21]. N. G. Khani, M. Abedi, G. B. Gharehpetian, and G. H. Riahy, “Offshore wind farm power control using HV dclink,” *Can. J. Electr. Comput. Eng.*, vol. 39, no. 2, pp. 168–173, 2016.
- [22]. S. Kurian, T. K. Sindhu, and E. P. Cherian, “Modelling and simulation of direct driven wind electric generator for grid integration,” in *Proc. Annu. IEEE India Conf. (INDICON)*, Kochi, India, Dec. 2012, pp. 171–174.
- [23]. S. Benelghali, M. E. H. Benbouzid, and J. F. Charpentier, “Comparison of PMSG and DFIG for marine current turbine applications,” in *Proc. 19th Int. Conf. Electr. Mach. (ICEM)*, Sep. 2010, pp. 1–6.
- [24]. C. Qin, P. Ju, F. Wu, Y. Jin, Q. Chen, and L. Sun, “A coordinated control method to smooth short-term power fluctuation of hybrid offshore renewable energy conversion system (HORECS),” in *Proc. IEEE Eindhoven PowerTech*, Jun. 2015, pp. 1–5.
- [25]. L. Wang and C.-N. Li, “Dynamic stability analysis of a tidal power generation system connected to an onshore distribution system,” *IEEE Trans. Energy Convers.*, vol. 26, no. 4, pp. 1191–1197, Dec. 2011.
- [26]. Chen, T. Tang, N. Ait-Ahmed, M. E. H. Benbouzid, M. Machmoum, and M. E.-H. Zaïm, “Attraction, challenge and current status of marine current energy,” *IEEE Access*, vol. 6, pp. 12665–12685, 2018.
- [27]. C. Y. Wang and L. Wan, “Type-2 fuzzy implications and fuzzy-valued approximation reasoning,” *Int. J. Approx. Reasoning*, vol. 102, pp. 108–122, Nov. 2018.